Vulnerability of Small Dams Subject to Induced Seismicity in Northeast British Columbia

Gennaro Esposito,
Dalhousie University, Halifax, NS, Canada
Gordon A. Fenton
Dalhousie University, Halifax, NS, Canada

GeoCalgary 2022 October 2-5
Reflection on Resources

ABSTRACT
Seismic events induced by rock fracturing for oil and gas extraction in Northeast British Columbia have generated concerns on the vulnerability of the existing structures in the area. The hazard caused by induced seismicity is non-stationary. In this work, we analyzed the seismic vulnerability of small dams located in the Kiskatinaw Seismic Monitoring and Mitigation Area (KSMMA). These dams are used to store water produced from gas extraction. We calculated the seismic hazard caused by the rock fracturing as a "short term – limited in space" hazard and then developed ground motion hazard curves for the region. The calculated ground motion hazard was the input of a probabilistic seismic slope displacement model that allowed the calculation of risk curves, representing the probability that the seismic strains experienced by the dams exceed the maximum strain of synthetic liners normally used for these structures.

RÉSUMÉ
Les événements sismiques induits par la fracturation des roches pour l'extraction de pétrole et de gaz dans le nord-est de la Colombie-Britannique ont suscité des inquiétudes quant à la vulnérabilité des structures existantes dans la région. L'aléa provoqué par la sismicité induite n'est pas stationnaire. Dans ce travail, nous avons analysé la vulnérabilité sismique de petits barrages situés dans la zone de surveillance sismique et d'atténuation de Kiskatinaw (KSMMA). Ces barrages sont utilisés pour stocker l'eau produite à partir de l'extraction du gaz. Nous avons calculé l'aléa sismique causé par la fracturation de la roche comme un aléa "à court terme - limité dans l'espace", puis nous avons développé des courbes d'aléa de mouvement du sol pour la région. Le risque de mouvement du sol calculé était l'entrée d'un modèle probabiliste de déplacement de pente sismique qui a permis le calcul de courbes de risque, représentant la probabilité que les contraintes sismiques subies par les barrages dépassent la contrainte maximale des revêtements synthétiques normalement utilisés pour ces structures.

1 INTRODUCTION

The recent increase of small to moderate induced seismic events in Northeast British Columbia has triggered the interest in the characterization of the vulnerability of structures and infrastructures in the region. Induced earthquakes are triggered by hydraulic rock fracturing (fracking) during oil and gas drilling and can generate ground motions of relatively large amplitude with usually short period of vibration at very small hypocentral distances.

This paper focusses on the vulnerability of many licensed produced-water hubs. A water hub is a facility where produced water or well fracture flowback is being stored from one or more well pads in an above-grade lined storage ponds enclosed by small dams. Some of the water hubs retain more than 30,000 m3 of fluid above grade and therefore are licensed by the regulator as dams, falling in the national dam regulation of the CDM (CDM, 2016).

Most of the available literature focusses on ground motion prediction equations (Atkinson et al., 2016), on the activation rate of seismicity for hydraulic fracture wells (Ghofrani and Atkinson, 2020), on regulation protocols based on either magnitude or human detection (Schultz et al., 2020), and on short term hindcast of the seismic hazard (Ghofrani et al., 2019). The authors of this work are not aware of any past and ongoing research aiming at deriving the ground motion hazard and vulnerability of engineered structures on the surface. The study presented in this paper aims at filling this gap considering the non-stationary nature of induced seismicity and its impact on water hubs. In detail, the objectives of this paper are a) to derive the short-term ground motion hazard related to the amount of fracking and b) to calculate the seismic vulnerability of water hubs conditional on the occurrence of fracking. The dam failure mode considered is the liner rupture caused by excessive deviatoric displacement of the dam.

2 STUDY AREA AND DAM GEOMETRY

The study area is the Kiskatinaw Seismic Monitoring and Mitigation Area (KSMMA – BC OGC, 2018) shown in Figure 1, which approximately covers an area of 60 km^2 including the towns of Fort St. John and Dawson Creek. In this area, there are seven licensed water hubs whose retained volume ranges from 60,000 to 200,000 m^3 of produced water. Many of these facilities use geomembrane liners to prevent water seepage through the berms and avoid the design of complicated seepage management systems. In this study we consider a water hub characterized by the height H of the assumed critical sliding mass (Figure 2) and the presence of the geomembrane liner on the interior side of the water hub. Usually, a cut-and-fill balance is used to build the water hub berms. Therefore, given the dominant surface geology, a mix of glaciolacustrine, glaciofluvial and alluvial soils are typically

excavated and placed at high Modified Proctor Relative Densities (90% and higher) to build the dam. Based on this, we assume that the mean shear wave velocity of the dam fill μ_{v_s} is 250 m/s. We also assume that a 1.5 mm (60 mil) Linear Low-Density Polyethylene (LLDPE) is the geomembrane liner system chosen for the water hub. We finally estimate the initial fundamental periods of the dam (Table 1) using the simplified approach of Bray and Travasarou (2007) as

$$T_s = 2.6H/\mu_{v_s} \quad [1]$$

We consider two heights H, 10 and 25 m and the resulting initial fundamental periods T_s are summarized in Table 1. Table 1 also shows the strength of the dam expressed in terms of the yield coefficient k_y (Bray and Travasarou, 2007). The yield coefficient k_y was estimated with conventional pseudo-dynamic slope stability analysis considering a berm fill friction angle of 29 degrees, a cohesion of 2 kPa, and a unit weight of 19 kN/m3.

Table 1. Characteristics of the modelled dams

Water Hub	H (m)	μ_{Vs} (m/s)	T_s (s)	k_y
A	10	250	0.12	0.2
B	25	250	0.26	0.15

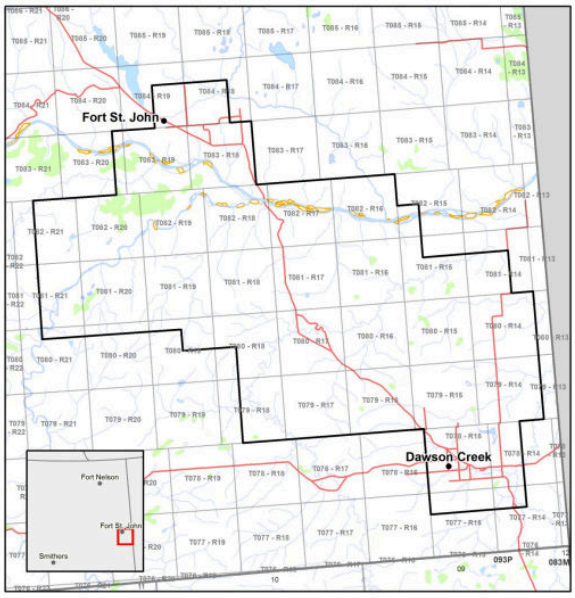

Figure 1. Kiskatinaw Seismic Monitoring and Mitigation Area (KSMMA) – BC OGC (2018)

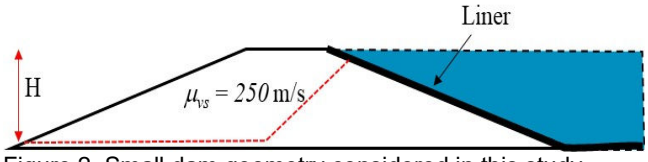

Figure 2. Small dam geometry considered in this study

3 DATA SELECTION

For the ground motion hazard, we adopt the framework developed by Teng and Baker (2020). Recent research has concluded that the hydraulic-fracturing-induced earthquakes tightly cluster around production wells in space and time (Atkinson et al., 2016; Schultz et al., 2018; Langenbruch et al., 2018; Wang et al., 2018, Hon 2021). Thus, the traditional seismic occurrence model, Poissonian mainshocks with non-stationary aftershock sequences, must be redefined (time limited) in order to compute short-term hazard levels near an active hydraulic fracturing operation (Teng and Baker, 2020). Moreover, hydraulic fracturing-induced earthquakes have small magnitudes, suggesting that their aftershocks should not have a significant contribution to the hazard level.

Based on the above observations, a short-term hazard level near a production site is defined as the rate λ of exceeding a ground motion intensity $S_a = a$ over the injection time interval, given injection activity as $\lambda(S_a \geq a|injection)$. During the injection time interval, usually days, we assume that the induced seismicity hazard is Poissonian. In this study, we use the spectral acceleration, S_a, at the initial fundamental period of the dam, T_s, as the measure of the ground motion intensity for the probabilistic slope stability analysis (Bray et al, 2007). For this purpose, we use the 2017-2018 earthquake catalogue published by NRCan (Visser et al., 2019) and select the events associated with production wells based on a spatiotemporal association filter modified from Schultz et al. (2018) as follows:

1. The earthquake occurrence time should be during the injection time period or within seven days of completion (hereafter referred to as the injection interval).
2. The earthquake epicenter should be within 10 km from the well surface location (Schultz et al., 2018).

4 PROBABILISTIC SEISMIC HAZARD ANALYSIS

Since for induced seismicity the source location is usually sufficiently close (within 2-3 km) to the injection pad, we assume that the epicenter coincides with the injection pad. The problem then becomes to predict the rate that, at a certain site located at the uncertain hypocentral distance r from the source, the ground motion intensity S_a exceeds a certain value a given the uncertain magnitude $M = m$ (Figure 3).

To calculate the rate λ of exceeding a ground motion intensity $S_a = a$ over the injection interval, given injection activity ($\lambda(S_a \geq a|injection)$), we modify the probabilistic model from Teng and Baker (2020) and first predict the number of earthquakes with magnitudes greater than M, induced during the injection interval using the following equation:

$$N(M_i \geq M|injection) = \delta_{HF} \cdot (10^a) \frac{10^{-b(M-M_c)} - 10^{-b(M_{max}-M_c)}}{1-10^{-b(M_{max}-M_c)}} \quad [2]$$

where δ_{HF} is the probability that the injection well is seismogenic. Figure 4 shows the spatial distribution of δ_{HF} for the studied area, showing that wells located in an almost horizontal strip between the towns of Fort St. John and Dawson Creek are more likely to induce earthquakes. In Eq. 2, 10^a is the number of earthquakes induced during the injection interval, Figure 5 shows the spatial distribution of a. Both δ_{HF} and a were estimated using kriging dividing the study area in cells having area equal to 150-by-150 m2 and using observed events in the KSMMA. The last term of Eq. 2 describes a Gutenberg-Richter distribution truncated between the magnitude of completeness M_c and the maximum considered magnitude M_{max}, where the b-value was taken as 1.37, following the results of Mahani (2020) that indicate a relative insensitivity of the b-value to the magnitude and the location in the study area. The magnitude of completeness is the minimum magnitude above which all earthquakes within a certain region are reliably recorded

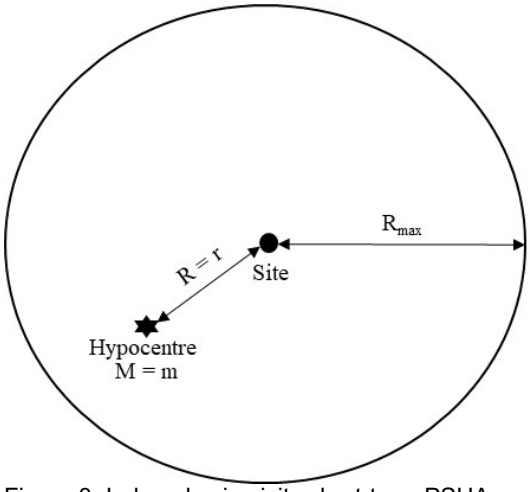

Figure 3. Induced seismicity short-term PSHA

In this study, we considered magnitudes truncated between 1.5 and 6.0 (where the upper limit was chosen for convenience, as increasing or decreasing it by a unit does not affect the results below). Note that the injection volume was excluded from the calculation. We are aware of other studies pointing to the possibility of correlation between injection volume and seismicity (Mahani et al., 2017), however regression analysis (not showed here) indicates that this is not the case in this region.

To define the short-term hazard, we considered a radius r_{max} of 10,000 m (10 km) around site and calculate the rate of exceeding a ground motion intensity S_a over the injection interval, given an injection, for a site at distance r. The calculation is repeated by source and by integrating over all possible magnitudes:

$$\lambda(S_a > a|injection) = \int_{M_c}^{M_{max}} \int_0^{R_{max}} P(S_a \geq a|m,r) \cdot f_R(r) \cdot N(M = m|injection) dr dm \quad [3]$$

where $P(S_a \geq a|m)$ is the probability of exceeding a ground motion intensity $A = a$ given a magnitude m earthquake, calculated using the ground motion prediction equation (GMPE) proposed by Atkinson (2015), $f_R(r)$ is the probability density function for the distance of a site from the hypocentre, and $N(M = m|injection)$ is the number of earthquakes with a magnitude of m during the injection interval, computed using Equation 2. We take $r_{max} = 10{,}000$ m as the GMPE predicts that at hypocentral distance larger than r_{max} the ground motion intensity is of no engineering interest. Also, we divide the KSMMA into a

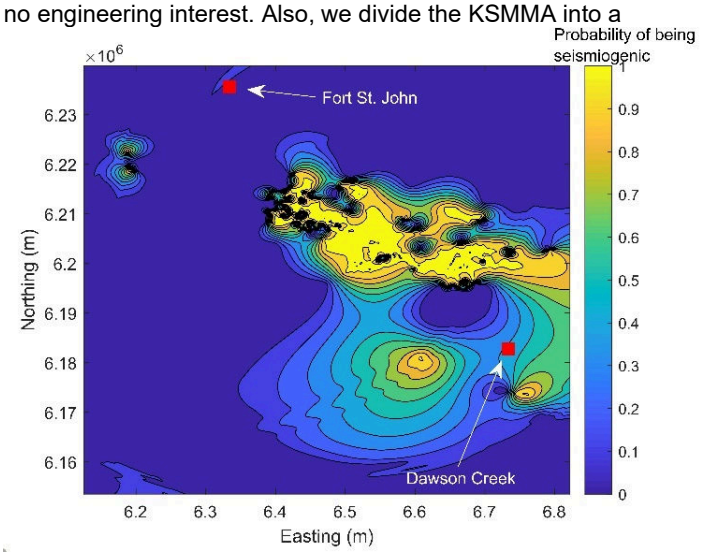

Figure 4. Spatial distribution of δ_{HF}

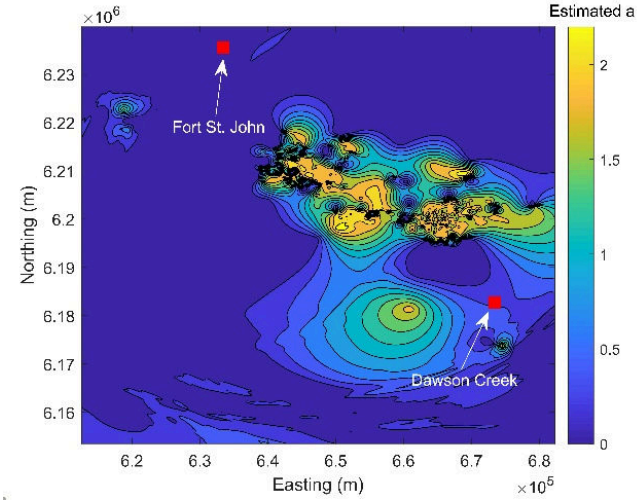

Figure 5. Spatial distribution of a.

grid of 150 by 150 m and apply Equation [3] at each node of the grid. With $r_{max} = 10{,}000$ m and considering equal likelihood in the area around the site, $f_R(r)$ can be written as

$$f_R(r) = \begin{cases} \frac{r}{r_{max}} & if\ 0 \leq r < 10{,}000 \\ 0 & otherwise \end{cases} \quad [4]$$

Finally, to solve Equation [3], we discretize our continuous distributions for *M* and *R*, and convert the integrals into discrete summations as

$$\lambda(S_a > a|injection) = \sum_{j=1}^{n_M} \sum_{k=1}^{n_R} P(S_a \geq a|m,r)P(M = m_j|injection)P(R = r_k) \quad [5]$$

We use this model for two sites of interests (Figure 6). Site A is in an area of high seismicity while site B is in an area of low seismicity. The resulting hazard is shown in Figures 7 and 8, which indicate that hazard at site B is low and that the dam vulnerability analysis at Site B is not of engineering interest. The seismic hazard is governed by the probability that the injection well is seismogenic, δ_{HF},. This is an important conclusion as the regulator should focus their attention in areas where δ_{HF} is at least 0.6-0.7. Seismic hazard curves calculated for other areas of the KSMMA (not shown in this paper) confirm the conclusion that induced seismic hazard of engineering interest is confined in the areas of the KSMMA region where δ_{HF} is at least 0.6-0.7.

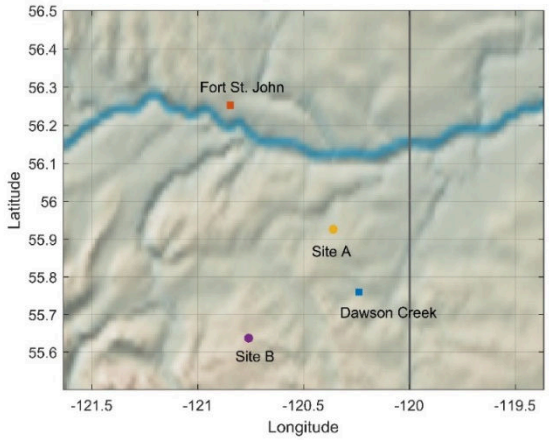

Figure 6. Locations showing where the induced seismic hazard is derived

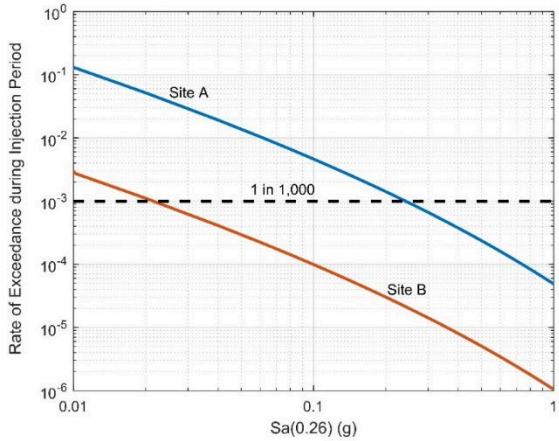

Figure 7. Seismic hazard for $S_a(0.26)$

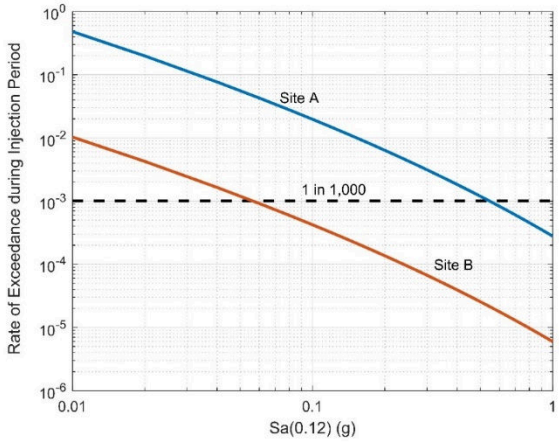

Figure 8. Seismic hazard for $S_a(0.12)$

5 SMALL DAM VULNERABILITY

To determine induced seismicity risk for the produced water ponds, we modify the approach of Macedo et al. (2017) which provides an explicit definition of the probability of negligible displacement and the median seismic-induced displacement. It models seismically induced permanent displacements as a mixed random variable that has a probability mass at "small" displacement (d_0) and a probability density for finite displacement values greater than d_0. Displacements smaller than d_0 are typically not of engineering significance and can, for all practical purposes, be considered to be negligible (i.e., zero). The values of seismic displacements that are smaller than d_0 are lumped together at d_0. The probability of "zero" displacements ($d \leq d_0$) and the median "non-zero" displacements are estimated based on the yield coefficient k_y, the initial fundamental period T_s, the spectral acceleration S_a at the fundamental period, and the moment magnitude M using ground motion recordings from shallow crustal earthquakes. More details are in Macedo et al. (2017).

The seismic displacement causing rupture of the liner and possible loss of containment corresponds to a dam displacement of 0.25 m (Rathje and Bray, 2011). For the vulnerability analysis, we derive the seismic displacement hazard curve for each injection, which defines the rate of the seismic displacement exceeding a specified seismic displacement threshold. This rate is given by (Macedo et al, 2018)

$$\lambda(D|injection) = \int_0^\infty P(D > d|S_a > a|injection)|d\lambda(S_a)| \quad [6]$$

where λ is the injection-related rate of exceedance; *D* is the seismic displacement; $S_a > a|injection$ is the intensity measure that characterizes the ground motion conditional to the injection, $P(D|S_a > a|injection)$ is the conditional probability of the seismic displacement exceeding d given S_a, and $|d\lambda(S_a)|$ is the absolute value of the derivative of the hazard curve for the selected intensity measure calculated with Eq. [5]. The conditional probability of the

seismic displacement is given in (Macedo et al, 2018). We modify the Macedo et al (2018) model by conditioning it for the occurrence of injection interval and eliminating the term regarding the deaggregation of the seismic hazard, since all the magnitudes generated by injection are relevant. This model is then incorporated in Eq. [6] to estimate the seismic displacement hazard. We finally estimate the probabilities of exceedance assuming that induced seismicity is Poissonian during the injection interval as (McGuire, 2004)

$$P(D|injection) = 1 - \exp\left[-\lambda(D|injection) \cdot T_{injection} \right]$$

Where $T_{injection}$ is the injection interval.

6 RESULTS OF VULNERABILITY ANALYSIS

The results of the vulnerability analysis are shown in Figures 9 and 10 for dam heights of 10 and 25 m respectively. The figures show the threshold displacement of 25 cm, from which the probability that the seismic displacement during the injection period exceeds 25 cm can be derived.

It is interesting to observe that 10 m high dams are more vulnerable than 25 m high dams. This is probably due to the Atkinson 2015 GMPE that predicts large ground motion hazard at short period, thus affecting small dams more than larger dams. For a 10 m high dam the probability that the seismic displacement exceeds 25 cm is 4 x 10-5, whereas for a 25 m high dam the probability that the seismic displacement exceeds 25 cm is 3 x 10-8, thus extremely small. Figure 9 and 10 also show the confidence intervals calculated as mean +/- 1 st. dev.. The probability that the upper bound seismic displacement exceeds 25 cm is 2 x 10-3 for a 10 high m dam and 7 x 10-6 for a 25 m high dam.

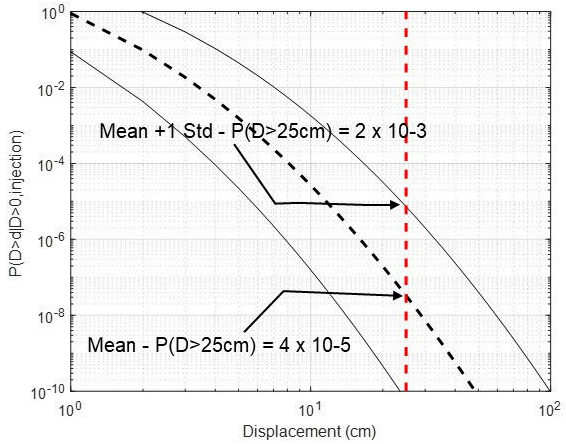

Figure 9. Hazard curve for 10 m high dam

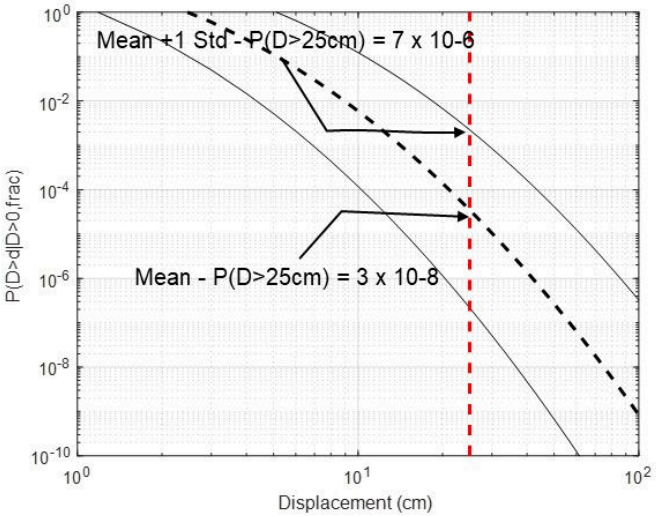

Figure 10. Hazard curve for 25 m high dam

7 CONCLUSIONS

From the analysis results presented in this paper, the following conclusions can be drawn:

- Seismic ground motion hazard of engineering interest occurs only in the areas where the probability of being seismogenic δ_{HF} is larger than 0.6-0.7.
- For the lined small dams with geometry and strength considered in this study exposed to one fracking operation, the probability that the displacement exceeds the limit of 25 cm is low, less than 10-3, when considering the predicted upper bound of the seismic displacement, and less than 10-4 when considering mean values of the displacement.
- Due to the larger ground motion hazard at low periods, typical of induced seismicity, smaller dams might experience larger seismic deviatoric displacements than larger dams, given the same strength and stiffness.

8 ACKNOWLEDGEMENTS

The financial support for this study given by BC OGRIS and the technical support to retrieve the earthquake data base offered by Natural Resources of Canada are gratefully acknowledged.

9 REFERENCES

Atkinson, G. M. (2015). Ground-motion prediction equation for small-to-moderate events at short hypocentral distances, with application to induced-seismicity hazards, Bull. Seismol. Soc. Am. 105, no. 2A, doi:10.1785/0120140142.

Atkinson, G. M., D. W. Eaton, H. Ghofrani, D. Walker, B. Cheadle, R. Schultz, R. Shcherbakov,

Bray, J. D., and Travasarou, T., 2007. Simplified procedure for estimating earthquake-induced deviatoric slope

displacements, Journal of Geotechnical and Geoenvironmental Engineering 133(4), 381–392.
Cornell, C. A. (1968). Engineering seismic risk analysis, Bull. Seismol. Soc. Am. 58, no. 5, 1583–1606.
Ghofrani, H., and G. M. Atkinson (2020). Activation Rate of Seismicity for Hydraulic Fracture Wells in the Western Canada Sedimentary Basin, Bull. Seismol. Soc. Am. XX, 1–20, doi: 10.1785/0120200002
Ghofrani, H., G. M. Atkinson, Schultz, R., (2019). Short-Term Hindcasts of Seismic Hazard in the Western Canada Sedimentary Basin Caused by Induced and Natural Earthquakes. Seismological Research Letters – doi: 10.1785/0220180285
Gupta, A., and J.W. Baker (2015). A Bayesian change point model to detect changes in event occurrence rates, with application to induced seismicity, 12th International Conference on Applications of Statistics and Probability in Civil Engineering, ICASP12, Vancouver, Canada, 8 pp.
Macedo, J., Bray, J., Abrahamson, N., Travasarou, T., (2017). Performance-Based Probabilistic Seismic Slope Displacement Procedure. Earthquake Spectra, DOI: 10.1193/122516EQS251M.
Mahani, Alireza & Schultz, Ryan & Kao, Honn & Walker, Dan & Johnson, Jeff & Salas, Carlos. (2017). Fluid Injection and Seismic Activity in the Northern Montney Play, British Columbia, Canada, with Special Reference to the 17 August 2015 M w 4.6 Induced Earthquake. Bulletin of the Seismological Society of America. 107. 10.1785/0120160175.
Mahani, Alireza B., (2020). Seismic b value within the Montney play of northeastern British Columbia, Canada. Canadian Journal of Earth Sciences. 58(8): 720-730. https://doi.org/10.1139/cjes-2020-0157
McGuire, R. K. (2004). Seismic Hazard and Risk Analysis, Earthquake Engineering Research Institute, Berkeley, California.
Rathje, Ellen & Bray, Jonathan. (2011). An examination of simplified earthquake-induced displacement procedures for earth structures: Reply. Canadian Geotechnical Journal. 37. 731-732. 10.1139/cgj-37-3-731.
Schultz, Ryan, Beroza, G. C., Ellsworth, W. L., and Baker, J. W. (2020). “Risk-informed recommendations for managing hydraulic fracturing induced seismicity via traffic light protocols.” Bulletin of the Seismological Society of America, 110(5), 2411-2422.
Teng, G., and Baker, J. W. (2020). “Short-term probabilistic hazard assessment in regions of induced seismicity.” Bulletin of the Seismological Society of America, 110(5), 2441-2453.
Visser, R., H Kao, B Smith, C Goerzen, B Kontou, RMH Dokht, (2019), A comprehensive earthquake catalogue for the Fort St. John–Dawson Creek region, British Columbia, 2017–2018, Tech. rep., Open File 8718, Geological Survey of Canada.